Influence of a future climate on the microphysical and optical properties of orographic cirrus clouds in ECHAM5

H. Joos,[1] P. Spichtinger,[1] and U. Lohmann[1]

[1]   The European Centre/Hamburg 5 (ECHAM5) general circulation model is used in order to investigate the influence of a warmer climate on the microphysical and optical properties of orographic cirrus clouds. The main goal of this study is to highlight the variety of processes influencing the formation of orographic cirrus and to emphasize the importance of coupling dynamics and cloud microphysics in order to provide realistic predictions of the influence of a future climate on cloud microphysical and radiative properties. Therefore, a coupling of gravity wave dynamics and cloud microphysics is implemented in the model. The influence of additional moisture on the propagation of gravity waves is investigated by using the dry and moist Brunt-Väisäla frequency in the calculation of the gravity wave-induced vertical velocity in two different simulations. In both simulations, the vertical velocities increase in the warmer climate. The additional moisture decreases the Brunt-Väisäla frequencies leading to less flow blocking and thus higher effective mountain heights. As this effect dominates over the decrease of the gravity wave amplitude due to more moisture, higher vertical velocities occur in a future climate. The opposite effect of a decreased vertical velocity in a future climate can be seen over the dry regions. From the present to the future climate, the ice crystal number concentration decreases despite the increased vertical velocities. Higher temperatures lead to a faster growth of the ice crystals, and the supersaturation is depleted faster such that no new crystals can be formed. The ice water content increases as more water vapor is available in a warmer climate. The net effect of a decreased ice crystal number concentration and an increased ice water content is an increased optical depth in a future climate. This result is in good agreement with recent cloud resolving studies. The effect of orographic cirrus clouds on the radiation is given by an increased short- and long-wave cloud forcing, whereas the latter dominates. However, from the present to the future climate, no changes in orographic cloud cover and cloud forcing over mountains can be seen.

1. Introduction

[2]   Cirrus clouds play an important role in the climate system. They cover approximately 30% of the Earth [*Wylie and Menzel*, 1999] and have a strong influence on the radiative budget. Depending on their microphysical properties like ice water content, ice crystal number concentration and cloud thickness, they can exert a cooling or warming on the Earth-atmosphere system. On the one hand, ice crystals scatter the incoming solar radiation back to space and thus cool the underlying atmosphere (albedo effect). On the other hand, ice crystals reduce the outgoing long-wave radiation and can lead to a warming (greenhouse effect). Generally, it is thought that the net effect of cirrus clouds is a warming [*Chen et al.*, 2000]. *Fusina et al.* [2007] showed that the transition from the cooling to the warming regime of a cloud is mainly determined by the ice crystal number concentration, which is determined by the vertical velocities. Updrafts induce adiabatic cooling and thus increase the relative humidity with respect to ice (RHi). If the critical threshold for homogeneous freezing is reached, a freezing event is initiated. This result emphasizes the importance of taking the correct dynamical processes for cirrus formation into account, in order to predict whether a cirrus cloud is warming or cooling.

[3]   As in most GCMs vertical velocities required for cloud formation are poorly represented, the cirrus cloud amount over continents is underestimated [*Dean et al.*, 2005; *Joos et al.*, 2008]. As shown by *Dean et al.* [2005] a substantial part of cirrus clouds over continents is formed due to orographic forcing. In orographic gravity

[1]Institute for Atmospheric and Climate Science, ETH Zurich, Zurich, Switzerland.

waves, high vertical velocities followed by the initiation of a freezing event can occur. Until now, there are only two GCMs available (HADAM3 and ECHAM5) which at least take the vertical velocities induced by orographic gravity waves and the formation of orographic cirrus into account [*Dean et al.*, 2005, 2007; *Joos et al.*, 2008]. *Dean et al.* [2007] parameterized the formation of orographic cirrus clouds by calculating a temperature perturbation due to subgrid-scale orographic gravity waves which can lead to the formation of ice. However, in this parameterization, only the ice water content can be influenced. *Joos et al.* [2008] explicitly calculate a vertical velocity induced by gravity waves which is used directly in the parameterization of the homogeneous freezing [*Kärcher and Lohmann*, 2002a]. Since in ECHAM5 a double-moment scheme for the ice phase is available, not only the ice water content but also the ice crystal number concentration is influenced by gravity waves. Reliable predictions of the microphysical properties of cirrus clouds and their influence on the radiative budget are only possible, if the ice water content as well as the ice crystal number concentration is simulated. In order to predict the future climate, the correct representation of cirrus clouds is crucial as a significant part of the uncertainties in the predicted climate change arises from the representation of these clouds [*Zhang et al.*, 2005]. In this paper we therefore present first estimates of changes in microphysical and optical properties of orographic cirrus clouds in a future climate and their impact on the radiative budget.

[4] *Joos et al.* [2009] performed simulations with the cloud resolving model EULAG [*Prusa et al.*, 2008] in order to show that there are dynamical and thermodynamical processes influencing the formation of orographic cirrus clouds which have to be considered. The vertical velocity induced by orographic gravity waves, which determine the ice crystal number concentration (ICNC), is expected to change in the future climate. The increase in moisture could lead to a dampening of the gravity wave amplitude and vertical velocities [see, e.g., *Durran and Klemp*, 1983; *Jiang*, 2003] followed by a decrease in ICNC and optical depth. Higher temperatures lead to a faster depositional growth of the crystals followed by a faster depletion of the supersaturation such that less crystals can form. Furthermore the increase in moisture and temperatures could lead to an enhanced ice water content (IWC) and optical depth. The net effect of these processes seems to be an increase in optical depth in the future climate as the increase in IWC dominates over the decrease in ICNC [*Joos et al.*, 2009].

[5] In order to investigate these effects on a global scale, simulations with the ECHAM5 global climate model [*Roeckner et al.*, 2003] are carried out. In section 2 we introduce the model and describe the new parameterizations of the orographic cirrus cloud cover and the reduced vertical velocity. Furthermore we introduce the moist Brunt-Väisäla frequency which is used in the calculation of the gravity wave induced vertical velocity. In section 3 we present the results of our simulations, and in section 4 we summarize our work and draw some conclusions.

2. Model Description

[6] In this chapter we describe the ECHAM5 model version used for this study. First, some key features which

are implemented in the standard version and which are crucial for the understanding of this work are explained. In section 2.2 we describe the additional parameterizations which were developed based on box model simulations and are implemented in the model in order to investigate orographic cirrus in a future climate.

2.1. The ECHAM Model

[7] In the version of ECHAM5 used here [*Lohmann et al.*, 2008], a two moment ice microphysics which calculates the ice water content and ice crystal number concentration is implemented. Homogeneous freezing of aqueous solution droplets is parameterized according to *Kärcher and Lohmann* [2002a]. The number of newly frozen ice crystals N_i^{hom} depends on a critical ice supersaturation S_{cr}, which only depends on temperature [*Koop et al.*, 2000], the water vapor number density at ice saturation n_{sat} and the vertical velocity w. The maximum number of ice crystals is limited by the number of hygroscopic aerosol particles. The number of newly frozen ice crystals can be approximated by the relationship

$$N_i^{hom} \propto w^{3/2} n_{sat}^{-1/2}. \tag{1}$$

Aerosol size effects for cirrus cloud formation are neglected here, as they were shown to be small [*Kärcher and Lohmann*, 2002b]. For cold temperatures and high vertical velocities, homogeneous freezing is thought to dominate [*Kärcher and Ström*, 2003]. Thus we focus on the homogeneous freezing mechanism in this study. However, we are aware that heterogeneous freezing could modify the microphysical properties of these clouds [*Spichtinger and Cziczo*, 2010; *Spichtinger and Gierens*, 2009b].

[8] The vertical velocity used in this parameterization consists of three parts. A large-scale, grid mean vertical velocity w_l, a contribution from the turbulent kinetic energy (TKE) w_t in order to represent subgrid-scale variations and a contribution from gravity waves w_{gw}. This gravity wave induced vertical velocity is calculated based on the linear theory for gravity waves and depends on the amplitude of the gravity wave δh, the horizontal wind speed U and wave number k. For a detailed description, see *Joos et al.* [2008]. The total vertical velocity used in this parameterization is then given by

$$w_{ges} = w_l + 0.7\sqrt{TKE} + kU\delta h = w_l + w_t + w_{gw}. \tag{2}$$

Due to the additional vertical velocity induced by gravity waves, the ice crystal number concentration in the upper troposphere over mountains could be enhanced quite substantial. As the vertical velocity seems to be overestimated, we neglect the contribution from the TKE whenever gravity waves occur. This leads to a better agreement of the vertical velocity with measured data [*Joos et al.*, 2008].

[9] In contrast to the version of ECHAM5 used by *Joos et al.* [2008], where the effective radius of ice crystals only depends on the ice water content, it is now parameterized such that it takes the influence of ICNC on the effective radius of ice crystals and thus the optical depth of ice clouds

into account. This parameterization calculates the mean volume radius R_v for clouds below $-35°C$ assuming spherical ice crystals. It is given by

$$R_v = \left(\frac{3 q_i \rho_a}{4 \pi \rho_i N_i}\right)^{1/3}, \qquad (3)$$

where q_i denotes the cloud ice mixing ratio in the cloudy part of the grid box in kg kg^{-1}, ρ_a is the air density, ρ_i is the ice density (925 kg m^{-3}), and N_i is the in-cloud ice crystal number concentration. For a more detailed description, see *Lohmann et al.* [2008]. The cloud optical depth is calculated for the short-wave (τ_{sw}) and long-wave (τ_{lw}) part of the spectrum and is given by

$$\tau_{sw} = f_i \kappa_i \text{IWP} \qquad \text{with} \qquad \kappa_i = a_0 R_i^{a_1}, \qquad (4)$$

$$\tau_{lw} = f_i \beta_i \text{IWP} \qquad \text{with} \qquad \beta_i = 1.66\left(a + \frac{b}{R_i}\right), \qquad (5)$$

where R_i is the effective radius of ice crystals in μm which is given by $R_i = R_v^3 (a_6 + b_6 R_v^3)$ with $a_6 = 1.61$ and $b_6 = 3.56 \times 10^{-4}$ [*Roeckner et al.*, 2003], $f_i = 0.85$ is a cloud inhomogeneity factor, κ_i is the mass extinction coefficient for ice clouds for the short-wave spectrum, with the parameters a_0, a_1 depending on the wave number, β_i is the mass absorption coefficient for the long-wave spectrum depending on the parameters a and b which vary with wave number and IWP is the ice water path in g m^{-2}. For the values of the parameters and a more detailed description, see *Roeckner et al.* [2003]. As the parameters for a_1 are negative, more and smaller ice crystals lead to an enhanced optical depth of ice clouds in the short-wave as well as the long-wave spectrum. With this parameterization we can investigate the influence of enhanced ICNC in orographic cirrus clouds due to a more realistic vertical velocity field on the radiation budget.

2.1.1. Moist Brunt-Väisälä Frequency in the Calculation of the Vertical Velocity

[10] In order to estimate the changes in microphysical and optical properties of orographic cirrus clouds in a future climate, we have to take the influence of moisture on the gravity wave dynamics into account. It has been shown in several studies [see, e.g., *Durran and Klemp*, 1983; *Jiang*, 2003], that additional moisture in the lower levels weakens the atmospheric stability and amplitudes of the gravity waves and thus the vertical velocity when the air is saturated. On the other hand, the windward flow stagnation can be delayed leading to higher effective mountain heights. *Surgi* [1989] implemented a gravity wave drag scheme [*Palmer et al.*, 1986] in the Florida State University Global Spectral Model in order to reduce the systematic errors. Additionally, the effect of moisture on the wave induced stress was incorporated by using the moist Brunt-Väisälä frequency instead of the dry Brunt-Väisälä frequency. Although the calculation of the moist Brunt-Väisälä frequency is very simple and the representation of the moisture field is poor in this model, the moist simulations showed better results than the corresponding dry simulations in reducing the systematic error. In order to make reliable predictions, we therefore need to consider the moist Brunt-Väisälä frequency N_m instead of the dry Brunt-Väisälä fre-

quency N_d in the calculation of the gravity wave amplitude and vertical velocity. The moist Brunt-Väisälä frequency N_m in ECHAM5 is calculated by substituting the potential temperature with the virtual potential temperature. It is given by

$$N_m^2 = \frac{g}{\theta_v} \frac{\partial \theta_v}{\partial z}, \qquad (6)$$

where θ_v is the virtual potential temperature given by

$$\theta_v = \theta(1 + 0.61 r - r_l - r_i), \qquad (7)$$

where $\theta = T(p_0/p)^{Rd/cp}$ is the potential temperature, r is the water vapor mixing ratio, and r_l and r_i are the liquid/ice water mixing ratios, respectively. The moist Brunt-Väisälä frequency N_m is then used in the calculation of the gravity wave induced vertical velocity $w_{gw} = kU \, \delta h$.

[11] The amplitude of the gravity wave δh_m calculated with N_m is given by

$$\delta h_m^2 = \frac{\rho_h N_{m_h} U_h Z_{eff}^2}{\rho N_m U}, \qquad (8)$$

where ρ is the density of air, U is the horizontal wind speed projected in the plan of gravity wave stress, and Z_{eff} is the effective height of the mountain that excites a gravity wave. The index h denotes values averaged between the surface, i.e., the altitude of the resolved orography Z_{mean} and the mountain peak. The effective height of the mountain Z_{eff} that excites gravity waves is calculated as,

$$Z_{eff} = \min\left(H_{nc} \frac{U}{N_m}, Z_{max} - Z_{min}\right). \qquad (9)$$

where H_{nc} is a critical nondimensional mountain height which is set to 0.5, Z_{max} is the peak height of the mountain and Z_{min} is the orographic valley elevation. For a more detailed description of the gravity wave induced vertical velocity and the flow blocking, see *Joos et al.* [2008]. As can be seen from equations (8) and (9), the consideration of the moist Brunt-Väisälä frequency N_m instead of the dry Brunt-Väisälä frequency N_d could change the effective mountain height and amplitude and hence the vertical velocity. An increase of moisture in a future climate could lead to a decrease of N_m. If this decrease is most pronounced in the low levels, the amplitude of the gravity wave decreases as well. However, the exact influence on the amplitude depends on the vertical profile of N_m. Changes in wind speed can additionally influence the vertical velocity. On the other hand, if N_m decreases, the effective mountain height Z_{eff} increases as the atmosphere is less stable and less flow blocking occurs. As shown by *Jiang* [2003], the addition of moisture causes a strong delay of windward stagnation and the critical mountain height for flow blocking increases substantially. This is equivalent with a higher effective mountain height as the flow blocking is reduced. We therefore might expect less flow blocking associated with larger effective mountain heights in a future climate. If the vertical velocity decreases or increases when N_m decreases depends on the overall effect of a higher effective mountain height, smaller

Table 1. Combinations of Horizontal Wavelength and the Associated Most Likely Occurring Maximum Vertical Velocities of Gravity Waves Occurring in ECHAM5

Wavelength (km)	Maximum Vertical Velocity (m s^{-1})
50	0.2, 0.5, 1, 1.5, 2, 3
100	0.2, 0.5, 1, 1.5, 2
150	0.2, 0.5, 1

gravity wave amplitudes and the changes in the horizontal wind speed.

2.2. Box Model Simulations

2.2.1. Parameterization of an Orographic Cirrus Cloud Cover

[12] In order to estimate the impact of orographic cirrus on the radiative budget, we developed a diagnostic parameterization for an orographic cirrus cloud cover, which is added to the standard cloud cover calculated in ECHAM5. For the simulations shown in this paper, we use the fractional cloud cover scheme originally developed by *Sundqvist et al.* [1989] and adopted by *Lohmann and Roeckner* [1996] where the fractional cloud cover b is an empirical function of relative humidity and given by

$$b = 1 - \sqrt{1 - b_0} \quad \text{with} \quad b_0 = \frac{r - r_0}{1 - r_0}, \quad (10)$$

where r is the grid-mean relative humidity and r_0 is a condensation threshold which is specified as a function of height. The variable r_0 is a tuning parameter, and the dependence on height was introduced to avoid excessive cloud formation in the lowest model level. For ice clouds, e.g., at temperatures below 235 K, the relative humidity with respect to ice is calculated. As ECHAM5 allows supersaturation with respect to ice, the cloud cover equals 1 if the air is supersaturated and a partial cloud cover is only calculated for sublimating ice clouds. The total cloud cover of cirrus clouds is newly calculated as the sum of b and an orographic cirrus cloud cover (OCC).

[13] The OCC parameterization is based on box model simulations. As a detailed ice microphysics is implemented in the model [*Spichtinger and Gierens*, 2009a], we can investigate the formation of ice in an air parcel, which follows a certain trajectory. In our case we selected a simple sine wave as this simple setup best represents the representation of orographic cirrus clouds in ECHAM5, where it is assumed, that in every grid box only one wave with a certain wavelength and vertical velocity occurs. With the box model we can investigate how long crystals can survive and thus how large the horizontal extent of the cloud is, when an air parcel follows this wave. We investigated this behavior for different initial RHi of the air parcel and for different horizontal wavelength and maximum vertical velocities. Table 1 shows which combinations of vertical velocity and wavelength most likely occur in ECHAM5. Based on these combinations we selected the setup for the box model. In all cases we simulated a distance of 400 km which is comparable to the maximum extension of a climate model's grid box. The box model version is able to treat

sedimentation of ice crystals in terms of an assumption about the ice mass/number flux through the top of the layer. It is assumed that a part of the flux through the bottom of the layer goes through the top, i.e., $F_{in} = f_{sed} F_{out}$, with a specified factor f_{sed}. For details see *Spichtinger and Cziczo* [2010]. Based on simulations of orographic cirrus clouds with the cloud-resolving model EULAG [*Prusa et al.*, 2008] including a detailed ice microphysics [*Spichtinger and Gierens*, 2009a], we estimated the ratio $f_{sed} = F_{in}/F_{out} = 0.9$. We also investigated the dependence of the results to the sedimentation by varying f_{sed} between 0 and 1. The overall picture of the results did not change, only for the extreme case of $f_{sed} = 0$ (strong sedimentation) the cloud extent was reduced substantially. Therefore, $f_{sed} = 0.9$ is used for all box model simulations.

[14] Figure 1 shows one example of a simulated sine wave with the corresponding evolution of temperature and vertical velocity. Here we show the results for $\lambda = 50$ km and a maximum vertical velocity of 1.5 m s^{-1}. We assume that the air undergoes one oscillation only as in ECHAM5 there is only one wave per grid box. After that the vertical velocity is set to zero and the temperature equals the initial temperature. Additionally, the evolution of the relative humidity and the formation of ice is shown.

[15] If the air parcel follows the sine wave its temperature cools down adiabatically and RHi starts to increase. If the critical threshold for homogeneous freezing is exceeded, crystals start to form and RHi is depleted by the growing ice crystals although the air parcel is cooled down further. The maximum ice water content is mainly determined by the initial RHi as it prescribes the amount of available water vapor. After the onset of the freezing event, the crystals start to grow and IWC increases. When temperature starts to increase again, the crystals start to evaporate and IWC decreases. However, if the crystals are large enough they do not evaporate completely such there is still ice left even after the parcel has passed the whole wave. The ice crystal number concentration (ICNC) that develops in the wave is determined by two factors. First, the vertical velocity at the time when the freezing starts, w_{nucl}, influences the ICNC. The higher the vertical velocity, the more crystals form. The second important factor is the temperature. At higher temperatures the depositional growth of the crystals is faster and the water vapor is depleted faster by the available ice crystals. Additionally, the ice nucleation rate is lower at higher temperatures. Therefore less new crystals can be formed. This can be seen in the curves for RHi = 70, 80, 90%. For these cases the vertical velocity w_{nucl} at freezing is nearly the same. However, ICNC decreases from RHi = 70% to RHi = 90%. This can be explained with the different temperatures at which ice crystals form. The temperatures decrease from 220.9 K for RH = 90% to 219.8 K for RH = 80% and T = 218.6 K for RH = 70%. Thus, for RHi = 90% the temperature when freezing starts is highest and ICNC is lower than for RHi = 70%/80%.

[16] Based on these simulations we calculated the horizontal extent of the cloud (see cldex in Figure 1). Depending on RHi, the crystals can survive the whole wave or are evaporated in the downdraft section of the cloud. We calculated the cloud extent for all combinations shown in Table 1 and for RHi = 50, 70, 80, 90, 100, 110, 120%. The results are shown in Figure 2. It can be seen that the horizontal
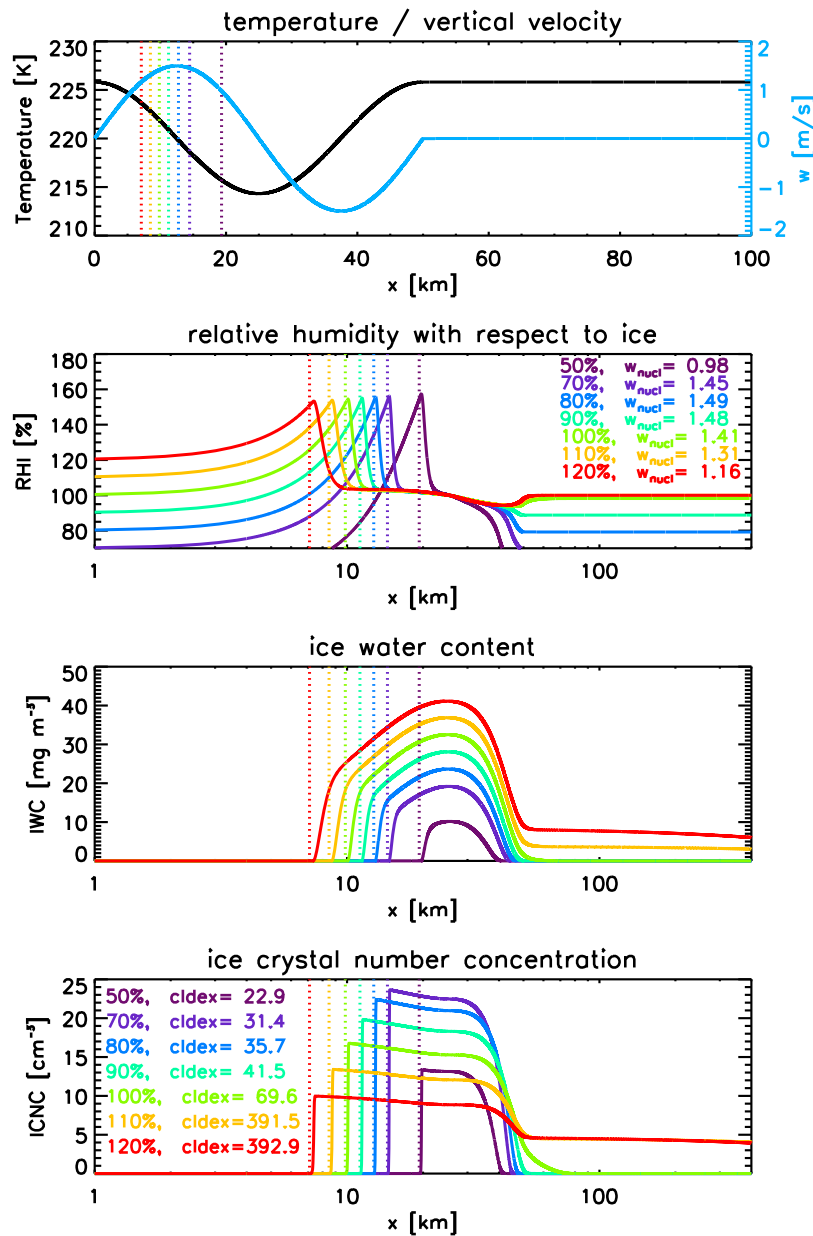
Figure 1. Simulated sine wave with corresponding temperature and vertical velocity, the evolution of RHi for different initial values, the ice water content, and the ice crystal number concentration. Please note that the x axes differ. Vertical lines indicate the time step when the freezing event starts. W_{nucl} denotes the vertical velocity at the time of the freezing event in m s^{-1}, and cldex denotes the cloud extent in km.

extent of the cloud does not depend on the vertical velocity at which the cloud formed. The cloud extent mainly depends on the initial relative humidity. If the initial RHi exceeds 100%, the crystals tend to survive the complete simulated distance of ~400 km. In a climate model this would mean that the whole grid box is covered by the cloud and the cloud cover would be 100%. However, if the RHi is smaller or equal 100%, the extent of the cloud equals in first approximation the wavelength λ of the wave. As we want to develop a very simple parameterization for the orographic cirrus cloud cover, we assume that the horizontal orographic cirrus cloud extent equals the wavelength of the gravity wave if the mean RHi in the grid box is lower than 100%. If

RHi exceeds 100% the whole grid box is covered and the cloud cover is set to 1. The advection of ice crystals which formed in an orographic wave over several hundreds of kilometers downstream is a realistic feature that can be observed [*Dean et al.*, 2007]. *Kay et al.* [2007] show that gravity waves generated over the Rockies affect cirrus cloud optical properties far downstream (Oklahoma). The OCC is given by

$$
\text{OCC} = \begin{cases} \dfrac{\lambda}{a(\phi)} & \text{if} \quad \text{RH}i \le 100\% \\ 1 & \text{if} \quad \text{RH}i > 100\% \end{cases}, \qquad (11)
$$
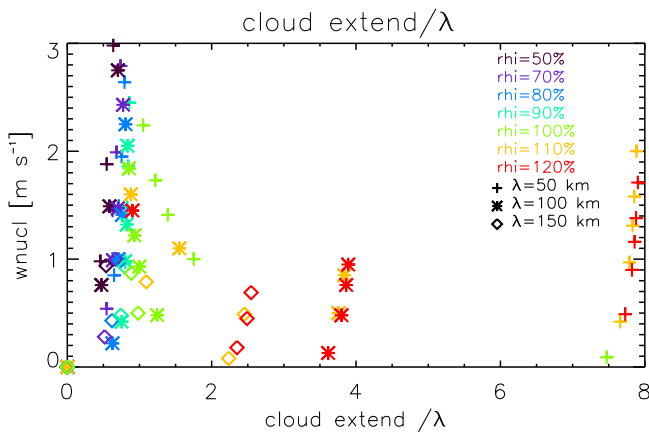
Figure 2. Horizontal cloud extent normalized with the wavelength as a function of w_{nucl} and RHi for $\lambda = 50$, 100, and 150 km. Colors indicate different initial RHi.

where a describes the horizontal extent of the grid box depending on the latitude φ. These calculations are only done if the temperature is below the threshold for homogeneous freezing and the vertical velocity induced by gravity waves w_{gw} is positive.

2.2.2. Reduction of the Vertical Velocity

[17] One interesting result of the box model simulations concerns the vertical velocity which influences the homogeneous nucleation (w_{nucl}). As can be seen very clearly in Figure 1, the vertical velocity which influences the freezing process and the ice crystal number concentration is not given by the maximum vertical velocity/cooling rate of the wave. It is rather the velocity which occurs at the moment when the critical threshold for homogeneous freezing is exceeded and nucleation starts. After the initiation of the first nucleation event, the supersaturation is depleted rapidly, such that no new crystals can form, although the air parcel is cooled down further with an even higher cooling rate until the maximum vertical velocity of the wave is reached. However, the onset of the freezing event inhibits a freezing event at the highest occurring vertical velocity. This "shadowing" effect is also mentioned by *Hoyle et al.* [2005]. They found that if the supersaturation is reduced significantly by the growing ice particles, all subsequent cooling rates are irrelevant, as the critical supersaturation for homogeneous freezing is not reached anymore.

[18] The vertical lines in Figure 1 denote the time when the critical threshold for homogeneous freezing is exceeded and the freezing event starts. As can be seen, this can happen before or after the maximum vertical velocity of the wave, depending on the initial relative humidity. When RHi = 120% the threshold is exceeded quite early and the homogeneous freezing starts at a vertical velocity w_{nucl} substantially lower than the maximum vertical velocity of the wave. On the other hand, if RHi = 50%, the critical threshold is only exceeded shortly before the minimum temperature is reached which also corresponds to a much lower w_{nucl} than the maximum vertical velocity.

[19] These simulations indicate that it is not the maximum vertical velocity occurring in the wave which is crucial for the freezing event. Similar results could also be seen in

cloud resolving simulations of orographic cirrus clouds [*Joos et al.*, 2009]. Based on the box model simulations, we therefore calculated a reduced vertical velocity which we implemented in the parameterization of the homogeneous freezing process in ECHAM5. At every grid box a sine wave with a certain amplitude, horizontal wavelength and maximum vertical velocity taken from the gravity wave scheme, is calculated. As the grid mean temperature and RHi is known, it is possible to calculate the RHi increase of an air parcel following the given sine wave, until a critical supersaturation is exceeded. The vertical velocity occurring at this moment is used as the reduced vertical velocity w_{nucl}. Until now, the maximum vertical velocity occurring in the gravity wave was used in this parameterization [*Joos et al.*, 2008]. However, this parameterization overestimated the occurring vertical velocities and ICNC when compared to measurements. This procedure is only carried out at grid points where gravity waves can be excited and when temperature is below $T = 235$ K such that the homogeneous freezing could occur. The new reduced vertical velocity is thus given by

$$w_{red} = w_l + w_{nucl}. \qquad (12)$$

3. Results

[20] Three different simulations were carried out in order to investigate the effect of a future climate on the microphysical and optical properties of orographic cirrus clouds. For all simulations we used a horizontal resolution of T63 which corresponds to 1.8×1.8 degree and 31 vertical levels using a time step of 12 min. The vertical resolution in the upper troposphere is about 30 to 40 hPa. We initialized the simulations with monthly mean SST and sea ice cover data, greenhouse gas concentrations and aerosol emissions (NIES) taken from an ECHAM5 IPCC A1B run [*Meehl et al.*, 2007]. The simulations are carried out for five years after a spin-up time of three months representative for the current climate (2002–2006) and the future climate (2091–2095). We performed one reference run (REF) and two additional simulations in which the reduced gravity wave induced vertical velocity w_{red} described by equation (12) and the OCC described by equation (11) are implemented.

[21] It is shown in several cloud resolving studies [*Durran and Klemp*, 1983; *Jiang*, 2003; *Muhlbauer and Lohmann*, 2008] that the addition of moisture strongly influences the propagation of gravity waves. In order to account for this effect in a global climate model we implemented the moist (N_m) and dry (N_d) Brunt-Väisälä frequencies in the calculation of w_{red} in the two additional simulations, in the following denoted as NDRY ad NMOIST, respectively. *Jiang* [2003] showed that the addition of moisture leads to less flow blocking and higher effective mountain heights. As this effect can only be calculated in the NMOIST simulation, we focus on this one in the following. Furthermore, *Surgi* [1989] shows that the incorporation of moisture in the calculation of the gravity wave induced stress lead to a larger reduction of systematic errors in a GCM as the corresponding dry simulation. In sections 3.1 and 3.2 we therefore focus on the difference between the NMOIST and REF simulations as we can take the effects described above
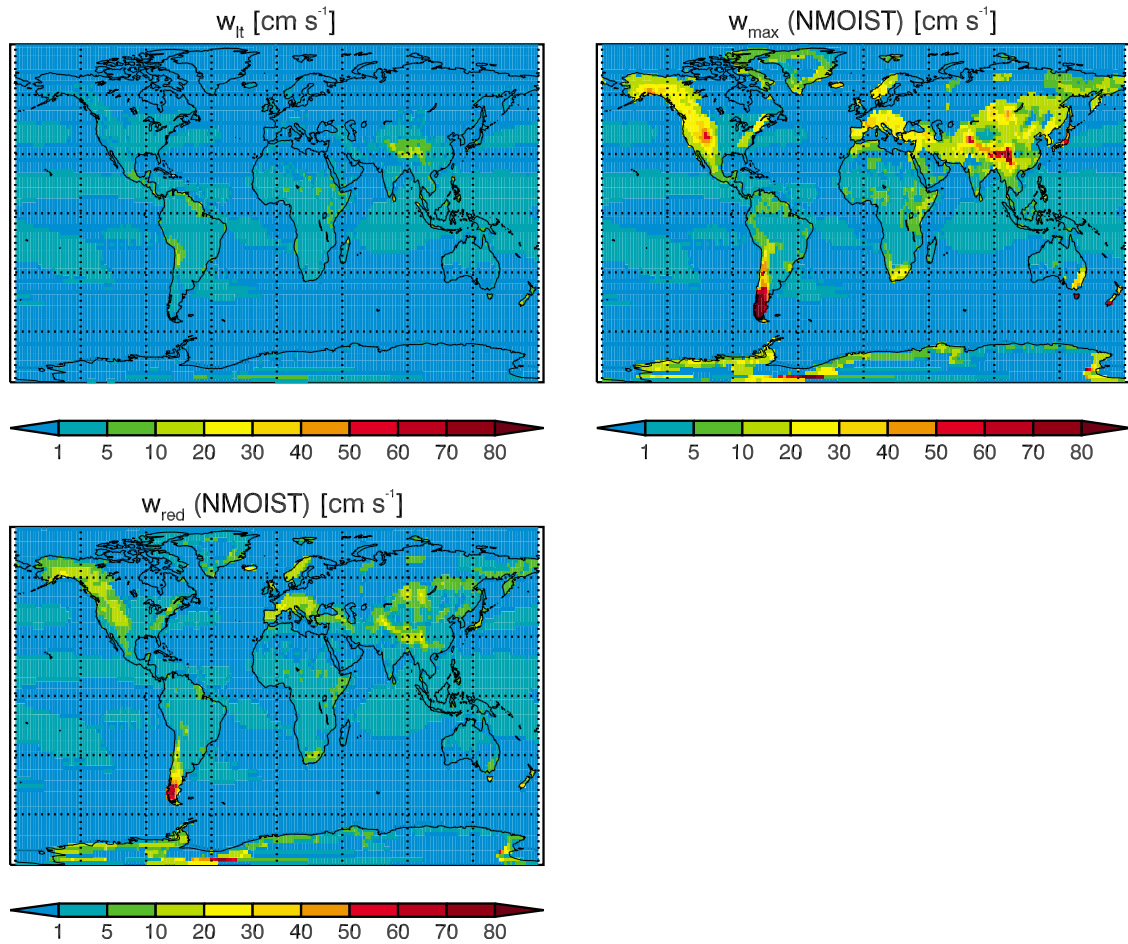
Figure 3. Five year mean vertical velocities as used in the parameterization of the homogeneous freezing process averaged over 165–285 hPa. The variable w_{lt} denotes the large-scale vertical velocity used in simulation REF, w_{max} denotes the vertical velocity with the maximum contribution from gravity waves (see equation (2)), and w_{red} denotes the reduced vertical velocity (see equation (12)) that is used in the homogeneous freezing parameterization. Note that there is no contribution from the TKE to w_{max} and w_{red} at the gravity wave active points.

into account in these simulations. Additionally, the differences between NDRY and NMOIST are discussed. In the following, we present the results for the present and future climate.

3.1. The Current Climate

[22] Simulations for the current climate with the three different model versions have been carried out. In the reference run (REF) the vertical velocity which influences the homogeneous freezing process consists of a large-scale part and a contribution from the turbulent kinetic energy $(w_l + w_t = w_{lt})$ whereas in the simulations NDRY and NMOIST, a gravity wave induced vertical velocity is also taken into account (see equation (12)). In Figure 3, the vertical velocities used in the parameterization of the homogeneous freezing process are shown. The results are averaged over the pressure range 165–285 hPa which refers to the model levels representing the upper troposphere. However, the results do not depend on the exact choice of the model levels. The large-scale vertical velocity w_{lt} used in REF (Figure 3, top left), is very small and amounts to <5 cm s^{-1} in most regions in the upper troposphere. The distribution

of vertical velocities changes completely if a contribution from orographic gravity waves is added. In the following, we show the results of NMOIST and REF. The results for NDRY are very similar and a detailed comparison of NDRY and NMOIST is shown in section 3.1.1. Over the high mountain ranges like the Rockies, the Andes, the Himalaya but also over New Zealand and Europe the vertical velocity is enhanced quite substantial and thus provides potential formation regions of orographic cirrus clouds. However, as mentioned earlier, it is not the maximum vertical velocity which is crucial for the freezing event. Therefore, the reduced vertical velocity w_{red} is shown in Figure 3 (bottom). It is much smaller than w_{max} over all mountains and shows that the critical relative humidity with respect to ice S_{cr} is reached and the homogeneous freezing starts in most cases long before or after the maximum vertical velocity of the wave is reached.

[23] The new vertical velocity has a strong influence on the microphysical properties. Figure 4 shows the absolute values for the REF simulations as well as the difference between NMOIST and REF for the ICNC, effective radius
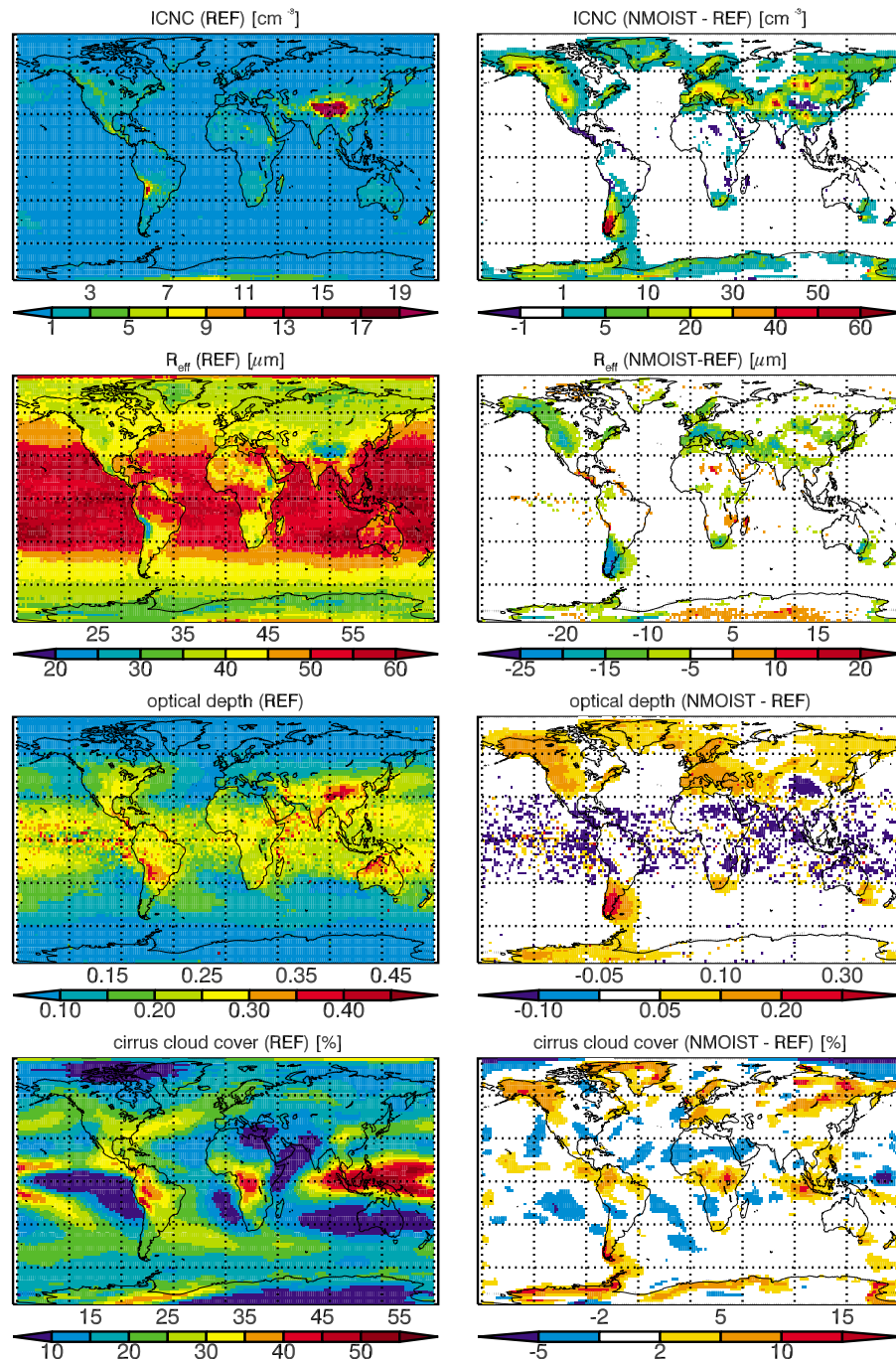
Figure 4. Absolute values of REF and difference between NMOIST and REF for a 5 year mean for the ICNC, the effective radius R_{eff}, the optical depth, and the cirrus cloud cover. All values are vertically averaged over 165–285 hPa.

R_{eff}, the optical depth sampled only over cloudy events and the cloudy part of the grid box and the cirrus cloud cover.

[24] As can be seen very clearly, the gravity wave induced vertical velocity leads to much higher ICNC over and in the lee of the big mountain ranges for example at the east coast of South America or New Zealand. The ice crystals form over the mountains but are advected downstream over several hundreds of kilometers. As shown by *Dean et al.* [2007], the advection of orographically induced ice crystals is a plausible mechanism of large-scale cirrus clouds downwind of major mountain ranges. Cloud resolving simulations by *Joos et al.* [2009] also show that orographically induced ice crystals can be advected over hundreds of kilometers. Thus, the advection of ice crystals over the adjacent ocean might be a realistic feature.

[25] As the calculation of the effective ice crystal radius depends on ICNC, R_{eff} decreases compared to the REF simulation especially over the continents where most crystals are formed. The ice water content (IWC) of the clouds also increases strongly as more crystals are nucleated which
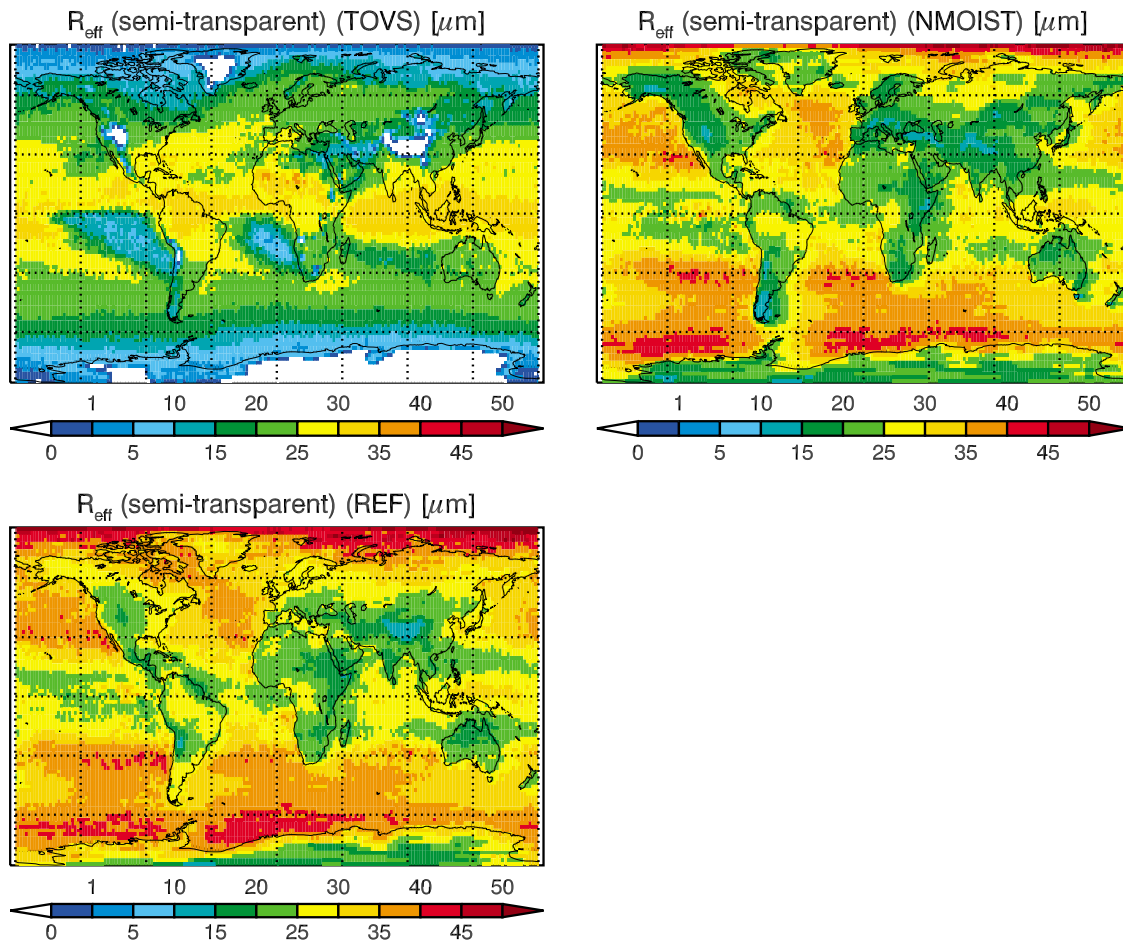
Figure 5. Comparison of observations from the TOVS satellite of R_{eff} for semitransparent cirrus (optical depth between 0.7 and 3.8) for the years 1988–1990 and a 5 year mean for the simulations REF and NMOIST.

can grow in contrast to REF where no or only a few crystals nucleate. As the growth is restricted to the available water vapor, more numerous but smaller crystals form in simulation NMOIST. Due to the smaller R_{eff}, the optical depth of the clouds increases (see equation (4)). Again the main feature is the enhanced optical depth over continents and downstream of the big mountains in NMOIST. As we added an additional cloud cover depending on the wavelength of the gravity wave whenever ice crystals formed due to gravity wave activity, the simulated cirrus cloud cover increases up to 10% over the gravity wave active regions and downstream. With this parameterization, the lack of cirrus clouds over continents as simulated with the ECHAM5 model and shown by *Joos et al.* [2008] can be reduced.

[26] Figure 5 shows the effective radius as measured by the TOVS satellite and the simulated radii. The effective radius as seen by the satellite is derived using data only for semitransparent cirrus clouds with an optical depth between 0.7 and 3.8 [*Stubenrauch et al.*, 2004]. In order to be able to compare the simulated and measured data, the same procedure is applied to the simulated values but the effective radius is not calculated in the same way from satellite observations and the ECHAM model. The main intention therefore is a qualitative comparison of the observed and simulated geographical pattern of the ice crystal effective radius. The satellite data of the effective ice crystal radius show a pattern with smaller ice crystals over the continents in the midlatitudes than over the oceans and larger radii in the tropics than in the midlatitudes. Especially over the large mountain ranges the crystals are smaller than in the surroundings. This can be seen, e.g., over the Rockies, the west coast of Scandinavia, the tip of South America and New Zealand. This pattern is not reproduced by the REF simulation. The radii in the tropics are smaller than in the midlatitudes and only a weak signal over high mountains can be seen. This signal is produced by the relatively high vertical velocities in these regions which arise from the contribution from the turbulent kinetic energy to the vertical velocity (see Figure 3). However, it is questionable if these vertical velocities are based on realistic physical processes. It is not surprising that the observed effective radius is not reproduced as it is not influenced by the correct dynamical processes which lead to the observed pattern. By taking the gravity waves in the freezing process into account, the simulated pattern can be improved. The simulation NMOIST shows a more distinct difference between ocean and land and it most notably produces smaller crystals over mountains. However, in general the simulated crystals in the tropics are too small. Over the midlatitudes oceans and especially around 60°S the crystal size is strongly over-
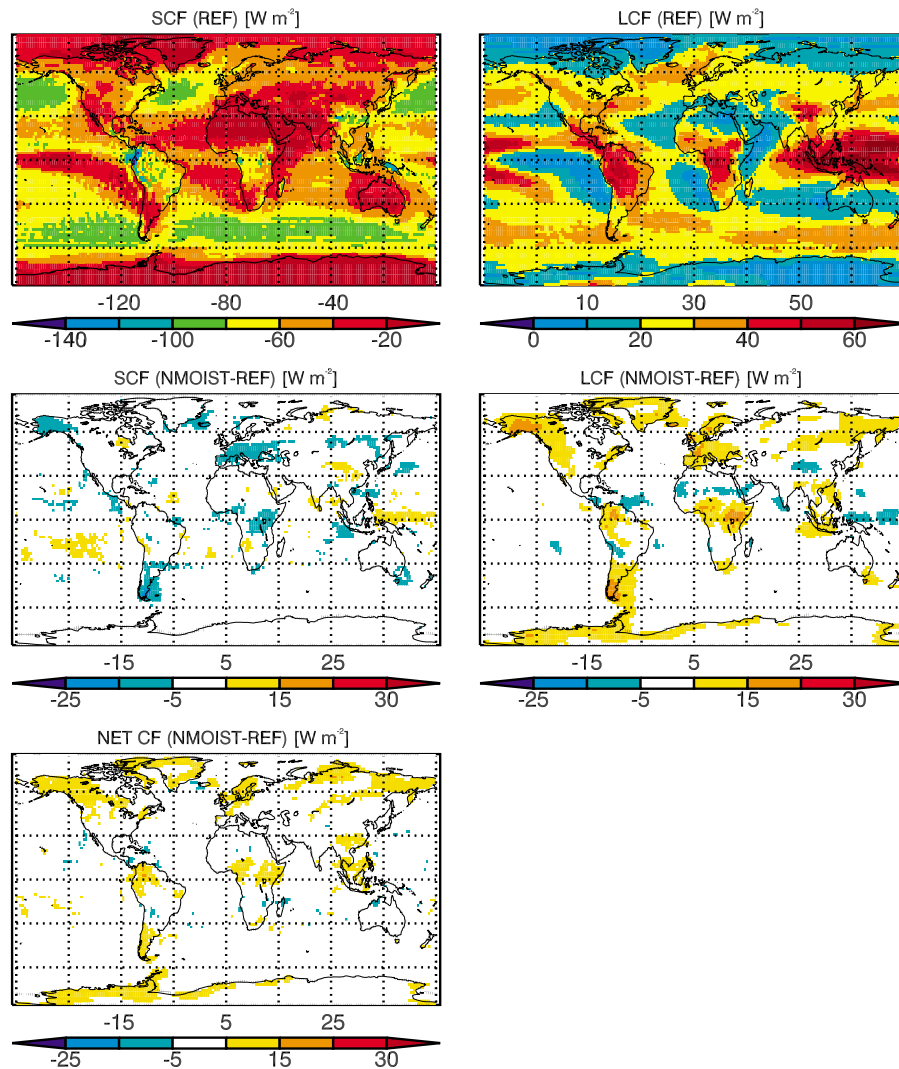
Figure 6. (top) Five year mean long-wave and short-wave cloud forcing for the REF simulation, (middle) the differences between NMOIST and REF, and (bottom) the difference in net cloud forcing between NMOIST and REF.

estimated. The implementation of gravity wave induced cirrus pushes the model results into the right direction. Thus, an improvement in the underlying dynamics allows simulation of more reliable microphysical properties. Especially the poor agreement over the oceans shows that further work is needed here to identify the dynamical processes which lead to the formation of cirrus clouds also over the oceans. Of course, an exact agreement cannot be expected here. The satellite data were measured from 1988 to 1990, whereas the model is representative for 2002–2006, but it could be shown that the general pattern can be reproduced better with the new parameterization.

[27] The changes in microphysical properties which lead to an enhanced optical depth influences the long-wave and short-wave radiation. Figure 6 shows the long-wave and short-wave cloud forcing for the REF simulation as well as the difference between NMOIST and REF and the difference in the net cloud forcing between NMOIST and REF. The difference between REF and NMOIST shows an increased SCF and LCF over the mountainous regions as

well as downstream of them. The increased ICNC, IWC and optical depth due to gravity wave activity thus influence the radiation budget in the short- and long-wave spectrum. As the optical depth of the orographic cirrus clouds is still small, LCF dominates over SCF in all regions (see net cloud forcing in Figure 6). LCF exceeds SCF especially in the high latitudes of the Northern Hemisphere. These are the regions where the most pronounced warming is expected in future [*Meehl et al.*, 2007]. The addition of orographic cirrus in climate projections would lead to an additional warming in these regions as more long-wave radiation is trapped.

[28] The changes in cirrus cloud microphysical and optical properties due to gravity wave activity might be overestimated. As shown by *Joos et al.* [2008], the simulated ICNC was overestimated as compared to measurements. In the model version used here, the depositional growth of ice crystals is slowed down as compared to the version used by *Joos et al.* [2008]. The depositional growth provides a sink for RHi and thus inhibits nucleation of even more crystals. Although in the version used for this study, we implemented
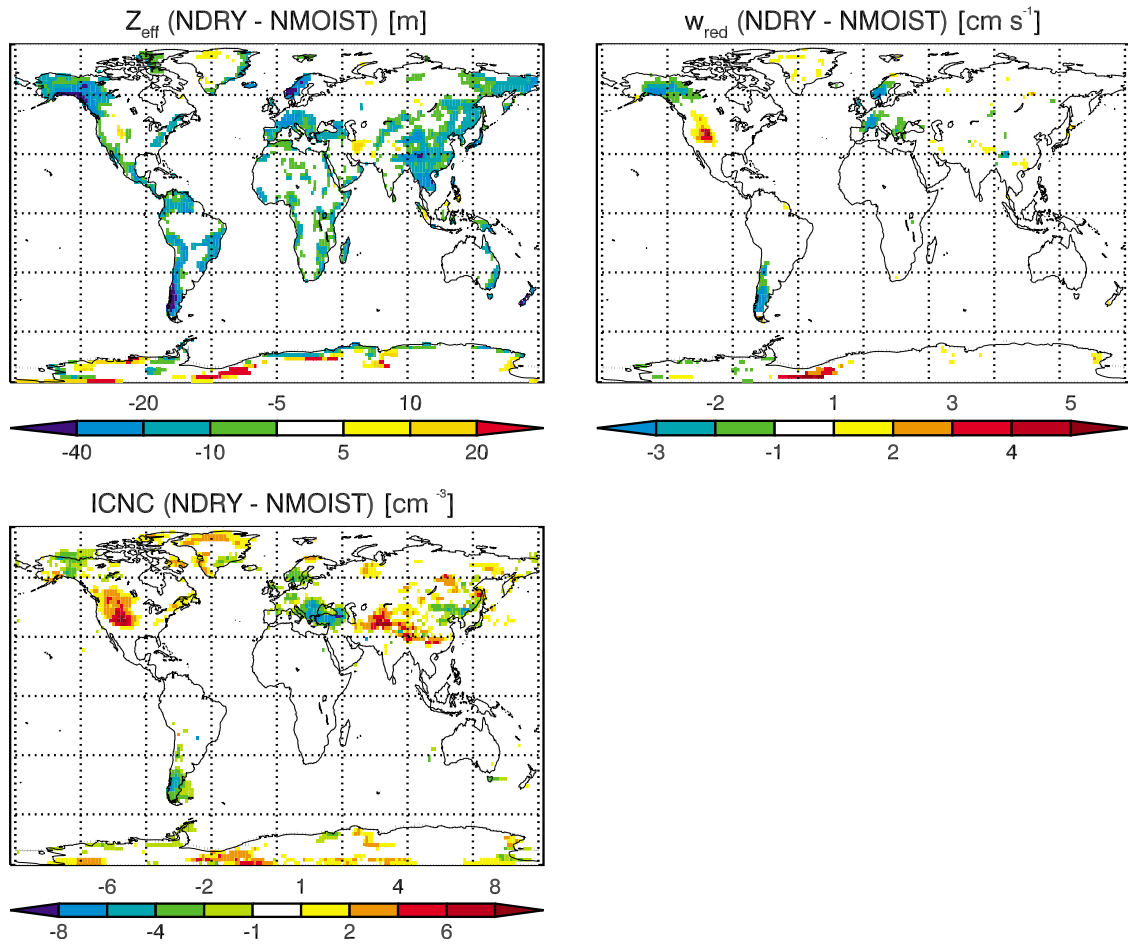
Figure 7. Difference NDRY-NMOIST for a 5 year mean of the effective mountain height Z_{eff}, the vertical velocities w_{red}, and the ICNC. The difference in w_{red} and ICNC shows a mean over the upper troposphere from 165 to 285 hPa.

a reduced vertical velocity in order to decrease the ICNC, we obtain more crystals which are caused by the slower depositional growth. Furthermore, changes in the sedimentation lead to smaller fall velocities such that the crystals stay longer in the atmosphere. This leads to the too high ICNC in the work presented here. However, the much more realistic formation of ice crystals using the underlying physical process provides a viable tool in order to estimate changes in the radiation budget especially in a future climate, although the absolute values might be overestimated.

3.1.1. Differences Between NDRY and NMOIST
[29] In order to take the influence of moisture on the propagation of gravity waves into account, an additional simulation with the dry Brunt-Väisälä frequency N_d in the calculation of the vertical velocity has been performed. The differences between NDRY and NMOIST are much smaller than between NMOIST and REF and are shown in Figure 7. If w_{red} in the NMOIST simulations is higher or lower compared to NDRY depends on the effective mountain height that excites the gravity waves and thus codetermines the amplitude of the gravity wave but also on the vertical wind and stability profile. The effective mountain height in turn depends on the horizontal wind speed as well as the Brunt-Väisälä frequency in the lowest model levels. A lower Brunt-Väisälä frequency leads to higher Z_{eff}, which

can lead to larger vertical velocities and vice versa if a constant horizontal wind speed is assumed. This effect can be seen in all continents. Thus, the pattern of the vertical velocity is partly determined by this effect. Over Alaska, the tip of South America and parts of Europe, the higher Z_{eff} in NMOIST leads to a higher w_{red}. However, as the vertical profile of the Brunt-Väisälä frequency and the wind speed also influences w_{red}, this effect cannot be seen everywhere and even the opposite effect of a higher w_{red} in NDRY occurs over parts of the United States. It can be seen that the changes in the effective mountain height are not necessarily the dominating process. The additional moisture can influence the gravity wave propagation in different and complex ways. Although the changes in the mean vertical velocity are weak, the ICNC is up to 8 cm^{-3} lower in the NMOIST simulation over a central part of the Rockies and the Himalaya. The opposite effect can be seen mainly over South America and southeast Europe.

[30] Based on these simulations, one can conclude, that the introduction of a moist Brunt-Väisälä frequency in the calculation of the gravity wave induced vertical velocity is justified. It increases the effective mountain height, which is a realistic effect and has also been shown by *Jiang* [2003], who showed that the critical mountain height for flow blocking increases substantially when moisture is added.
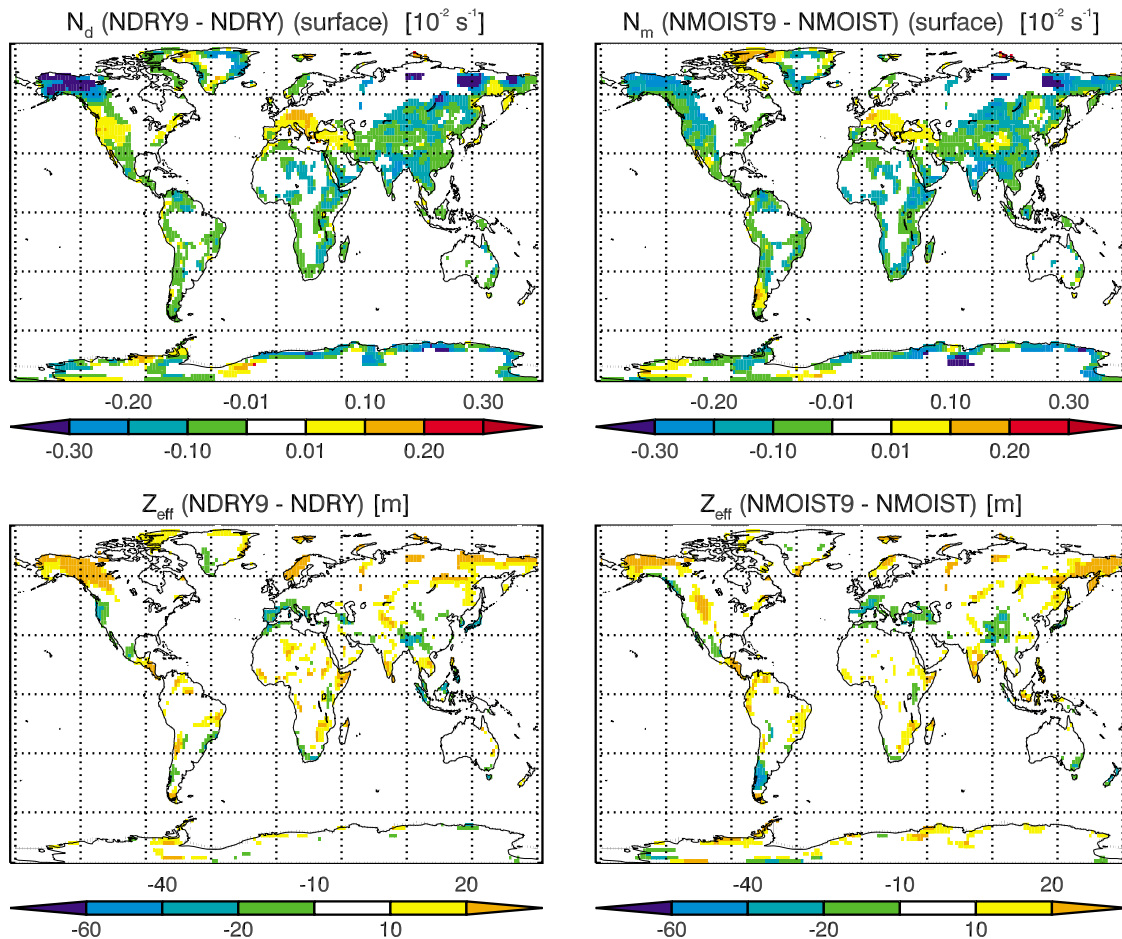
Figure 8. Difference between (top) the future and current climate of the Brunt-Väisälä frequency at the surface and (bottom) the effective mountain height.

Depending on the changes in the vertical moisture and wind profiles this leads to an increase/decrease in the vertical velocity and thus reduces/enhances the ICNC on a regional scale. This is especially important with regard to the future climate where changes in specific humidity could influence the propagation of gravity waves and thus the formation of orographic cirrus.

3.2. A Future Climate

[31] The three simulations REF, NDRY and NMOIST have also been performed for a future climate (hereafter REF9, NDRY9, NMOIST9). The simulations were initialized with the sea surface temperature, sea ice cover, greenhouse gases and aerosols representative for the years 2091–2095. Aerosol emissions are taken from the Japanese National Institute for Environmental Studies (NIES) (T. Nozawa, NIES, personal communication, 2004) and sea surface temperature and sea ice were taken from the CERA database from an ECHAM A1B simulation. In the future climate simulations the global mean surface temperature increases from 289 K in REF to 291.7 K in REF9. In this section we show the differences between the current and a future climate as well as the differences between NDRY9 and NMOIST9 in order to estimate the effect of moisture on orographic gravity waves and cirrus clouds.

[32] The differences in the REF simulation between the current and future climate are relatively weak concerning the microphysical properties of ice clouds (not shown here). ICNC over continents decreases slightly due to a slight decrease in the vertical velocity whereas over the oceans no differences can be seen. Furthermore the ice water content (IWC) increases slightly as in a warmer climate there is more water vapor available for the formation of ice and the ice crystals become bigger especially in the tropics and the storm tracks. However, the changes especially over the continents are much smaller than the changes occurring in NDRY and NMOIST. In the orographic gravity wave active regions we can conclude that the changes are mainly influenced by the gravity waves and do not occur in the REF simulation.

[33] Figure 8 shows the difference between the future and current climate in the Brunt-Väisälä frequency at the surface and the corresponding effective mountain height. Over many regions, Z_{eff} increases in the future climate in the NDRY as well as the NMOIST simulation. This is caused by a destabilization at the surface leading to lower N and higher Z_{eff}. However, there are also regions where N_m and N_d increase and Z_{eff} decreases. These regions correspond to regions which are very dry and where a drier climate/desertification is expected in future like southwest United States/northern Mexico, southern Europe and the southern
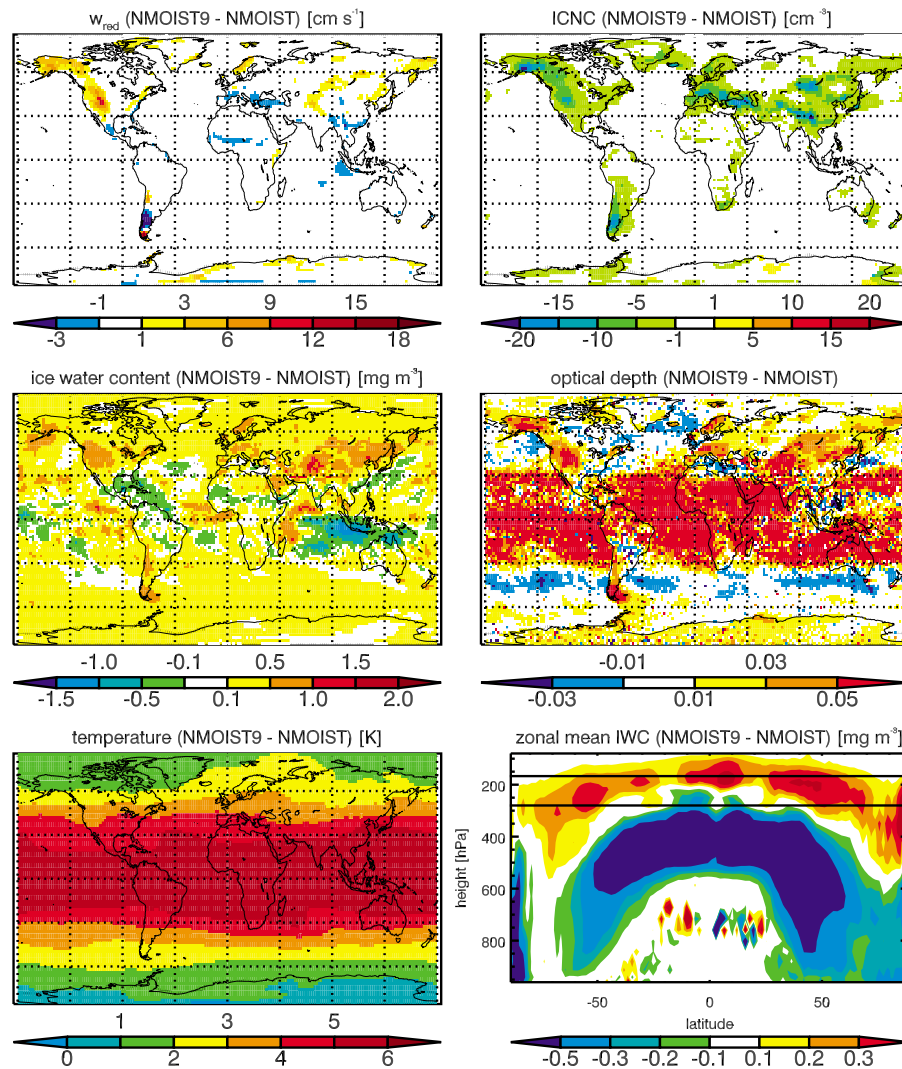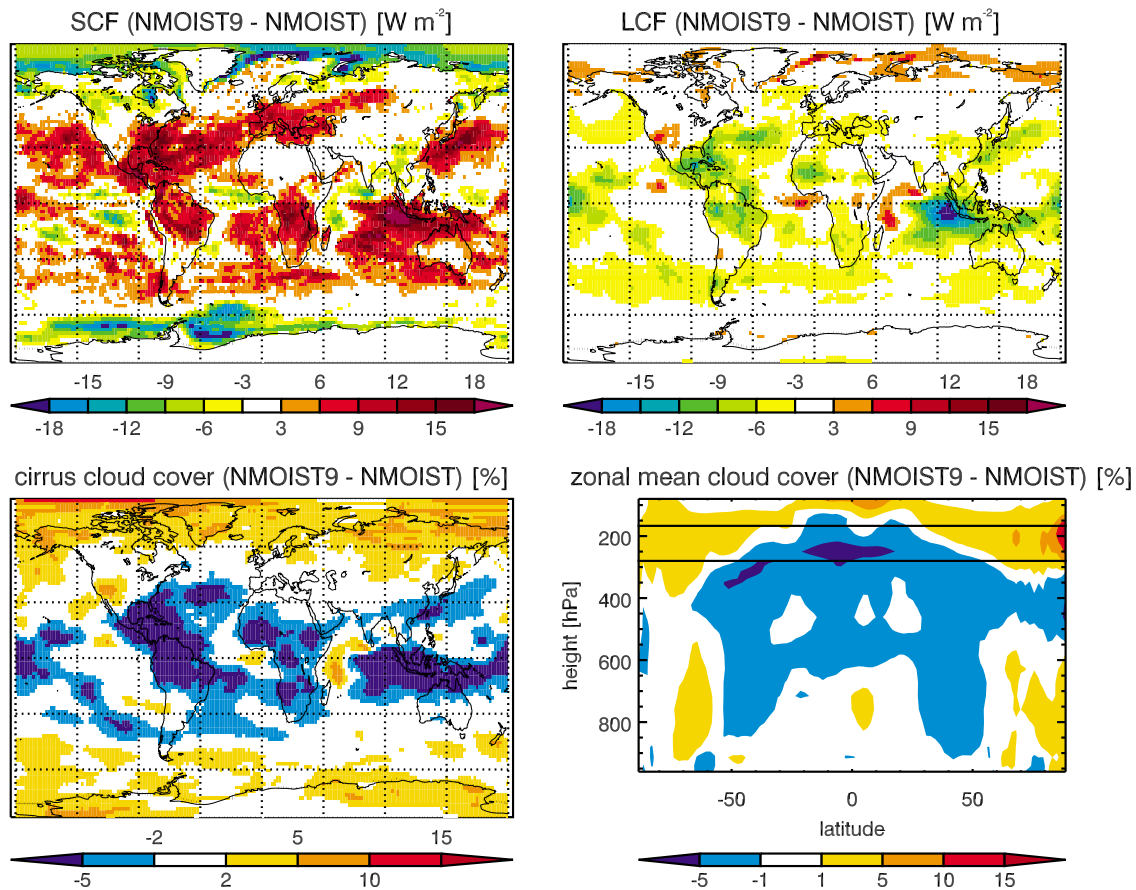
Figure 9. Difference between NMOIST9 and NMOIST for the reduced vertical velocity w_{red}, the ICNC, IWC, cloud optical depth sampled only over cloudy events, and temperature. All values are averaged over 165–285 hPa, representative for the upper troposphere. Additionally, difference between NMOIST9 and NMOIST for the zonal mean IWC is shown. Black lines denote 165 and 285 hPa.

part of South America [*Christensen et al.*, 2007; *Meehl et al.*, 2007]. The pattern of N and Z_{eff} further determines the changes in the vertical velocity and the microphysical properties of the cirrus clouds.

[34] Figure 9 shows differences between the NMOIST9 and NMOIST simulation for vertical velocity, ice crystal number concentration, ice water content, optical depth, temperature and a zonal mean of the ice water content. Over most of the mountain ranges, the vertical velocity increases from the present to the future climate. This effect is most pronounced over the Rockies, the tip of South America, Scandinavia and New Zealand. As mentioned above, this is caused by a decrease of the moist Brunt-Väisäla frequency at the surface in this regions leading to less flow blocking followed by a higher effective mountain height. The opposite effect of a more stable atmosphere in a future climate with higher Brunt-Väisäla frequencies, smaller Z_{eff} and w_{red} can be seen, e.g., over southern South America and southern Europe. These are again the regions where a drier climate is

expected in future. The results for the NDRY9 simulation are very similar. These results point out that the development of drier regions at the surface could influence the high cirrus clouds due to changes in the dynamics.

[35] Interestingly, ICNC decreases from the present to the future climate in contrast to the vertical velocity. Despite higher vertical velocities, fewer ice crystals are formed. At warmer temperatures, the depositional growth is faster. It depends on the diffusivity of water vapor in air. The higher the temperature, the higher is the diffusivity leading to a faster growth of the crystals such that the supersaturation is depleted faster and no new crystals can be formed. This temperature effect dominates over the dynamical changes leading to a lower ICNC of up to 20 cm^{-3} over the Rockies, Central Europe and the Himalaya. At the same time, as more water vapor is available in the warmer climate, IWC increases, especially over the mountain ranges and in the midlatitudes. Less ice crystals would lead to a smaller optical depth of ice clouds, whereas an increased IWC leads

Figure 10. Difference between NMOIST9 and NMOIST for the LCF, SCF, total cloud cover averaged over 165–285 hPa, and zonal mean of total cloud cover. Black lines denote 165 and 285 hPa.

to an enhanced optical depth of ice clouds. The net effect on the optical depth of ice clouds in the short-wave spectrum can be seen in Figure 9 (middle right). The optical depth increases slightly over the major mountain ranges in the midlatitudes from the current to the future climate. At the tip of South America it increases even in the lee of the Andes meaning that the ice crystals are advected further due to higher wind speeds in the future climate. In the tropics, the signal is weaker. Due to the temperature increase in a future climate, the formation of ice clouds is shifted to higher altitudes (see Figure 9, bottom right). This effect is most pronounced in the tropics where the temperature increase is strongest. At the same time, the liquid water content (LWC) increases. As the optical depth is influenced by both the LWC and IWC, it increases in the tropics in our considered pressure range (285–165 hPa). As there is no increase in LWC in the midlatitudes, the simulated increase in optical depth is caused by the increased IWC there. The effect of an increased optical depth of ice clouds in a future climate has also been seen in the cloud resolving simulations shown by *Joos et al.* [2009]. A decrease in ICNC due to warmer temperatures and relatively small dynamical changes combined with an increased IWC as more water vapor is available also lead to higher optical depth for the warmer climate in these simulations.

[36] The difference of LCF/SCF, total cloud cover and the zonal mean cloud cover between the current and future climate is shown in Figure 10. The change in cirrus cloud cover over mountains is very small. This is mainly caused by the fact that in both cases (NMOIST and NMOIST9) many crystals form and the frequency of occurrence of an orographic cirrus cloud cover does not change. In the tropics, the high cloud cover decreases in future due to a vertical shift of the clouds to higher altitudes (see Figure 10, bottom right) but in general, no pattern which could be caused by orographic cirrus can be seen. The increased optical depth of ice clouds in future should influence the LCF/SCF. However, the LCF/SCF is influenced by all clouds and the pattern of the LCF/SCF is dominated by the differences in the total cloud cover (not shown) instead of changes in microphysical properties of ice clouds. Furthermore, as the orographic cirrus cloud cover does not change, no signal from these clouds can be expected here. For a better investigation of the influence of cirrus on the radiation budget it is necessary to improve the parameterization of the cirrus cloud cover. The cloud cover parameterization used here calculates a partial cloud cover above $RHi > 70\%$ and 100% cloud cover if $RHi > 100\%$ and deposition occurs. Given that supersaturation is required before homogeneous nucleation can occur, RHi always exceeds 100% when the cloud forms. Thus a partial cloud cover for cirrus could only occur for sublimating cirrus when RHi drops below 100%. This is far too simple and prevents a realistic investigation of the radiative effect of changes in orographic cirrus cloud

Table 2. Global Mean Long-Wave Cloud Forcing, Short-Wave Cloud Forcing, and the Net Cloud Forcing for All Simulations[a]

Simulation	LCF (W m^{-2})	SCF (W m^{-2})	NCF (W m^{-2})
OBS	21.6 to 30	−46.6 to −50	−20 to −17
REF	26.8	−51.3	−24.5
NMOIST	28.1	−51.6	−23.5
NDRY	28.1	−51.9	−23.8
REF9	23.8	−48.6	−24.8
NMOIST9	25.4	−49.3	−23.9
NDRY9	25.4	−49.2	−23.8

[a]The observations (OBS) of SCF, LCF, and net cloud forcing (NCF) are taken from *Kiehl and Trenberth* [1997] . In addition, estimates of LCF from TOVS retrievals [*Susskind et al.*, 1997; *Scott et al.*, 1999] and SCF retrievals from CERES [*Kim and Ramanathan*, 2008] are shown.

cover in a future climate. The main features described here also occur in the NDRY simulations. The differences between NDRY9 and NMOIST9 are described in more detail in section 3.2.1.

[37] The differences between the NMOIST9 and REF9 simulations (not shown here) show the same behavior as for the current climate. Due to the increased vertical velocity in NMOIST9 the ICNC is higher than in REF9 leading to an increased optical depth, IWC and cirrus cloud cover over mountains. However, the difference in ICNC is smaller than for the current climate as less crystals form in NMOIST9 compared to NMOIST due to warmer temperatures and changes in the reference simulations are negligible. However, the difference in IWC is higher for the future as more water vapor is available and thus can be transferred to the ice phase. This leads to a higher difference in the optical depth in the future (NMOIST9-REF9) than in the current climate (NMOIST-REF).

[38] Table 2 summarizes the long-wave and short-wave cloud forcing for all simulations. The introduction of orographic cirrus clouds increases LCF and SCF as compared to the reference version of the model both in the current and the future climate (compare NMOIST versus REF and REF9 versus NMOIST9) whereby the increase in LCF is more pronounced. The net cloud forcing is thus less negative in the simulations containing orographic cirrus compared to the REF simulations in better agreement with observations

(see Table 2). The difference in LCF/SCF from the current to the future climate is dominated by changes in cloud cover in general and not by the orographic cirrus clouds (see Figure 10).
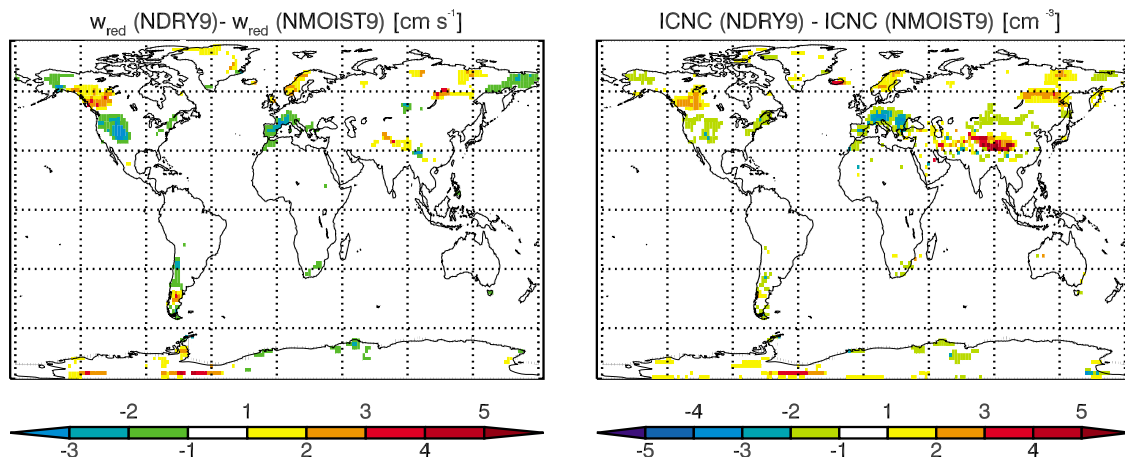
3.2.1. Differences Between NDRY9 and NMOIST9

[39] In order to assess the difference in orographic cirrus clouds depending on whether N_m or N_d is used for the calculation of the gravity wave induced vertical velocity, the simulations NDRY9 and NMOIST9 are described here in more detail.

[40] In the warmer climate in the ECHAM5 simulation, the air contains more humidity leading to a decrease of N_m. This decrease is strongest in high latitudes of the Northern Hemisphere as there the warming and the following increase in moisture is most pronounced, but also in the tropics a decrease can be seen (see Figure 8). These changes influence the vertical velocity as the vertical propagation of gravity waves is influenced. In order to assess the differences between NDRY9 and NMOIST9, Figure 11 shows the differences in the vertical velocity and ICNC. Over most of the globe, the differences between the two simulations are negligible. In some regions, differences in the vertical velocity and ICNC can be seen. However, the inter annual variability lies in the same order of magnitude. Furthermore, the complex interaction of additional moisture, changes in vertical profiles of the Brunt-Väisäla frequency and the horizontal wind speed do not allow to interpret the results in regard to changes in ICNC caused by the influence of moisture on the propagation of gravity waves and hence the vertical velocity.

[41] In general, the differences between the current and future climate are much larger than the differences between NDRY9 and NMOIST9 and go in the same direction for both simulations. However, this analysis might be a hint, that it could be important to consider the influence of moisture on the dynamics in order to be able to make realistic predictions for the future climate. This effect could be important at least at a regional scale.

[42] Based on these results it is very hard to determine which one of these simulations is more realistic. The effect of an increased effective mountain height caused by a destabilization due to more moisture is a realistic effect.

Figure 11. Difference between NDRY9 and NMOIST9 of (left) the vertical velocity and (right) the ICNC. All values are averaged over 165–285 hPa.

However, the behavior of gravity waves in a future climate has to be investigated in more detail in order to make reliable conclusions about the development of orographic cirrus in a warmer climate. This study only presents possible mechanisms and points out that the influence of the dynamics on the cirrus cloud formation is an important factor and should be taken into account in global climate models in future studies.

4. Summary and Conclusions

[43] The ECHAM5 GCM has been used in order to investigate the influence of orographic cirrus clouds on the radiative budget in the current and future climate. The implementation of a coupling of gravity wave dynamics with ice microphysics as described by *Joos et al.* [2008] and a two moment ice microphysics implemented in the standard ECHAM5 allows estimation of the effect of gravity waves on the microphysical and optical properties of cirrus clouds. In contrast to the version of ECHAM5 used by *Joos et al.* [2008] several changes have been applied in the model version used here.

[44] First, instead of using the maximum vertical velocity of a gravity wave for the homogeneous freezing process, we now use a reduced vertical velocity. It represents the vertical velocity occurring at the moment when the supersaturation with respect to ice for the first time exceeds the critical value S_{cr} which is needed for the homogeneous freezing process. This procedure reduces the vertical velocity substantially as in most cases, S_{cr} is reached either long before or after the maximum vertical velocity in the gravity wave is reached. As also shown by, e.g., *Hoyle et al.* [2005] the vertical velocity at the moment when freezing commences determines the ice crystal number concentration. With the maximum vertical velocity we would overestimate ICNC. Thus, the new reduced vertical velocity presents an improvement as it better represents the physical processes.

[45] Second, a cloud cover for orographic cirrus clouds has been implemented. Based on box model simulations, the horizontal extent of orographic cirrus clouds has been determined depending on the relative humidity with respect to ice, the vertical velocity and the horizontal wavelength of the gravity wave. This implementation increases the cirrus cloud cover over the big mountain ranges of up to 10% and thus reduces the lack of cirrus cloud cover over these regions shown by *Joos et al.* [2008]. Furthermore, in the used model version, the optical depth of ice clouds depends on the effective radius of the ice crystals which in turn depend on ICNC. This enables us to investigate the influence of a changed ICNC on the radiative budget. However, we have to mention here that the cirrus cloud cover scheme is a relative humidity based scheme which assumes a cloud cover of 100% whenever cirrus form in an environment that is supersaturated with respect to ice. As this is clearly an oversimplification, it is essential to implement a cloud cover parameterization which takes into account the processes mentioned before in order to be able to make reliable predictions of the influence of cirrus clouds in general on the radiation budget.

[46] Furthermore, we investigated the effect of a warmer moister climate on the propagation of gravity waves and the following influence on the vertical velocity and ICNC.

Therefore, in one simulation the moist Brunt-Väisälä frequency is implemented in the calculation of the gravity wave induced vertical velocity, whereas in the other one, the dry Brunt-Väisälä frequency is used.

[47] The main intention of this study is to highlight the complex interaction of the influence of moisture on the dynamics and the coupling of dynamics, cloud formation and microphysics. Our results show that in order to simulate realistic changes in the microphysical and radiative properties, it is crucial to take all these processes and feedbacks into account. Due to the uncertainties in the microphysical parameterizations we do not want to give a quantitative estimation of the radiative impact of orographic cirrus clouds in a future climate.

[48] The results for the present-day climate show an increase in the vertical velocity in the NDRY and NMOIST simulation compared to REF. This causes more numerous but smaller ice crystals over the big mountain ranges followed by a higher optical depth of the clouds. Furthermore, the cirrus cloud cover is enhanced between 5 and 15% in these regions. The comparison of the effective radius to satellite data shows that the pattern with smaller crystals over continents is better represented in NDRY and NMOIST although the model is not able to simulate realistic effective radius over oceans. The comparison of the short- and long-wave cloud forcing between NMOIST and REF shows that the long-wave effects dominate as the optical depth is still relatively small. Especially at high latitudes, LCF increases compared to REF. The implementation of orographic cirrus clouds could thus amplify the predicted warming in these regions which is already expected to be the highest in a future climate.

[49] The differences between NDRY and NMOIST show a higher effective mountain height in NMOIST over most mountain ranges, caused by smaller Brunt-Väisälä frequencies leading to less flow blocking. The distribution of the vertical velocities mainly follows the pattern of the effective mountain height.

[50] For the future climate, the vertical velocity increases over most of the mountains again caused by a decreased stability in the warmer climate followed by an increased Z_{eff}. However, over the dry regions which are expected to get even drier in future, the opposite effect can be seen. This is a very interesting result as it shows that a desertification could influence cirrus clouds as the dynamics might change. ICNC decreases from the current to the future climate although the vertical velocity increases. Higher temperatures and a faster depositional growth compensate the dynamical changes. As more water vapor is available in a future climate, IWC and the optical depth of ice clouds increase. The effect of an increased optical depth of cirrus clouds has also been shown in cloud resolving simulations [*Joos et al.*, 2009]. The good agreement of the cloud resolving and global simulations might be seen as a hint that an increased optical depth of orographic cirrus clouds in future climate could be a realistic feature.

[51] As the orographic cirrus cloud cover almost stays the same in the simulations NMOIST and NMOIST9, hardly any changes in the radiative budget can be seen over the mountains. However, as the parameterization of cirrus cloud cover is not realistic in ECHAM, it is hard to estimate the effect of the changed optical depth of the orographic cirrus

on the radiative budget in a future climate. This result again emphasizes the importance of a realistic cirrus cloud cover parameterization in order to estimate the influence on radiation.

[52] In general, the warmer climate leads to an increased optical depth of cirrus clouds in NDRY9 and NMOIST9. Which of the simulations is more realistic cannot be determined at the moment and is not the intention of this study. However, these results point out that on a regional scale it is important to take the influence of moisture on the gravity wave dynamics into account as it might change the microphysical and optical properties of cirrus clouds substantially. However, it might be questionable if the GCM with its low vertical resolution has the ability to simulate these effects realistically, but it can at least provide information on which processes might occur and should be investigated further.

References

Chen, T., W. Rossow, and Y. Zhang (2000), Radiative effects of cloud-type variations, *J. Clim.*, *13*, 264–286, doi:10.1175/1520-0442(2000)013<0264:REOCTV>2.0.CO;2.

Christensen, J., et al. (2007), Regional climate projections, in *Climate Change 2007: The Physical Science Basis. Contribution of Working Group I to the Fourth Assessment Report of the Intergovernmental Panel on Climate Change*, edited by S. Solomon et al., pp. 847–940, Cambridge Univ. Press, Cambridge, U. K.

Dean, S., B. Lawrence, R. Grainger, and D. Heuff (2005), Orographic cloud in a GCM: The missing cirrus, *Clim. Dyn.*, *24*, 771–780, doi:10.1007/s00382-005-0020-9.

Dean, S., J. Flowerdew, B. Lawrence, and S. Eckermann (2007), Parameterization of orographic cloud dynamics in a GCM, *Clim. Dyn.*, *28*, 581–597, doi:10.1007/s00382-006-0202-0.

Durran, D., and J. Klemp (1983), A compressible model for the simulation of moist mountain waves, *Mon. Weather Rev.*, *111*, 2341–2361, doi:10.1175/1520-0493(1983)111<2341:ACMFTS>2.0.CO;2.

Fusina, F., P. Spichtinger, and U. Lohmann (2007), The impact of ice supersaturated regions and thin cirrus on radiation in the mid latitudes, *J. Geophys. Res.*, *112*, D24S14, doi:10.1029/2007JD008449.

Hoyle, C., B. Luo, and T. Peter (2005), The origin of high ice crystal number densities in cirrus clouds, *J. Atmos. Sci.*, *62*, 2568–2579, doi:10.1175/JAS3487.1.

Jiang, Q. (2003), Moist dynamics and orographic precipitation, *Tellus, Ser. A*, *55*, 301–316, doi:10.1034/j.1600-0870.2003.00025.x.

Joos, H., P. Spichtinger, U. Lohmann, J.-F. Gayet, and A. Minikin (2008), Orographic cirrus in the global climate model ECHAM5, *J. Geophys. Res.*, *113*, D18205, doi:10.1029/2007JD009605.

Joos, H., P. Spichtinger, and U. Lohmann (2009), Orographic cirrus in a future climate, Atmos. *Chem. Phys.*, *9*, 7825–7845, doi:10.5194/acp-9-7825-2009.

Kärcher, B., and U. Lohmann (2002a), A parameterization of cirrus cloud formation: Homogeneous freezing of supercooled aerosols, *J. Geophys. Res.*, *107*(D2), 4010, doi:10.1029/2001JD000470.

Kärcher, B., and U. Lohmann (2002b), A parameterization of cirrus cloud formation: Homogeneous freezing including effects of aerosol size, *J. Geophys. Res.*, *107*(D23), 4698, doi:10.1029/2001JD001429.

Kärcher, B., and J. Ström (2003), The roles of dynamical variability and aerosols in cirrus cloud formation, *Atmos. Chem. Phys.*, *3*, 823–838, doi:10.5194/acp-3-823-2003.

Kay, J. E., M. Baker, and D. Hegg (2007), Physical controls on orographic cirrus inhomogeneity, *Atmos. Chem. Phys.*, *7*, 3771–3781, doi:10.5194/acp-7-3771-2007.

Kiehl, J., and K. Trenberth (1997), Earth's annual global mean energy budget, *Bull. Am. Meteorol. Soc.*, *78*, 197–208, doi:10.1175/1520-0477(1997)078<0197:EAGMEB>2.0.CO;2.

Kim, D., and V. Ramanathan (2008), Solar radiation budget and radiative forcing due to aerosols and clouds, *J. Geophys. Res.*, *113*, D02203, doi:10.1029/2007JD008434.

Koop, T., B. Luo, A. Tsias, and T. Peter (2000), Water activity as the determinant for homogeneous ice nucleation in aqueous solutions, *Nature*, *406*, 611–614, doi:10.1038/35020537.

Lohmann, U., and E. Roeckner (1996), Design and performance of a new cloud microphysics scheme developed for the ECHAM general circulation model, *Clim. Dyn.*, *12*, 557–572, doi:10.1007/BF00207939.

Lohmann, U., P. Spichtinger, S. Jess, T. Peter, and H. Smit (2008), Cirrus cloud formation and ice supersaturated regions in a global climate model, *Environ. Res. Lett.*, *3*, doi:10.1088/1748-9326/3/4/045022.

Meehl, G., et al. (2007), Global climate projections, in *Climate Change 2007: The Physical Science Basis. Contribution of Working Group I to the Fourth Assessment Report of the Intergovernmental Panel on Climate Change*, edited by S. Solomon et al., pp. 747–845, Cambridge Univ. Press, Cambridge, U. K.

Muhlbauer, A., and U. Lohmann (2008), Sensitivity studies of the role of aerosols in warm phase orographic precipitation in different dynamical flow regimes, *J. Atmos. Sci.*, *65*, 2522–2542, doi:10.1175/2007JAS2492.1.

Palmer, T., G. Shutss, and R. Swinbank (1986), Alleviation of a systematic westerly bias in general circulation and numerical weather prediction models through an orographic gravity wave drag parameterization, *Q. J. R. Meteorol. Soc.*, *112*, 1001–1039, doi:10.1002/qj.49711247406.

Prusa, J., P. Smolarkiewicz, and A. Wyszogrodzki (2008), EULAG, a computational model for multiscale flows, *Comput. Fluids*, *37*, 1193–1207, doi:10.1016/j.compfluid.2007.12.001.

Roeckner, E., et al. (2003), *The atmospheric general circulation model ECHAM5. Part I: Model description*, Rep. 349, Max Planck Inst. for Meteorol, Hamburg, Germany.

Scott, N., A. Chedin, R. Armante, J. Francis, C. Stubenrauch, J. Chaboureau, F. Chevallier, C. Claud, and F. Cheruy (1999), Characteristics of the TOVS pathfinder path-b data set, *Bull. Am. Meteorol. Soc.*, *80*, 2679–2702, doi:10.1175/1520-0477(1999)080<2679:COTTPP>2.0.CO;2.

Spichtinger, P., and D. Cziczo (2010), Impact of heterogeneous ice nuclei on homogeneous freezing events in cirrus clouds, *J. Geophys. Res.*, *115*, D14208, doi:10.1029/2009JD012168.

Spichtinger, P., and K. Gierens (2009a), Modelling of cirrus clouds: Part 1a: Model description and validation, *Atmos. Chem. Phys.*, *9*, 685–706, doi:10.5194/acp-9-685-2009.

Spichtinger, P., and K. Gierens (2009b), Modelling of cirrus clouds: Part 2: Competition of different nucleation mechanisms, *Atmos. Chem. Phys.*, *9*, 2319–2334, doi:10.5194/acp-9-2319-2009.

Stubenrauch, C., F. Eddounia, and G. Rädel (2004), Correlations between microphysical properties of large-scale semitransparent cirrus and the state of the atmosphere, *Atmos. Res.*, *72*, 403–423, doi:10.1016/j.atmosres.2004.03.024.

Sundqvist, H., E. Berge, and J. Kristjansson (1989), Condensation and cloud parameterization studies with a mesoscale numerical weather prediction model, *Mon. Weather Rev.*, *117*, 1641–1657, doi:10.1175/1520-0493(1989)117<1641:CACPSW>2.0.CO;2.

Surgi, N. (1989), Systematic errors of the FSU global spectral model, *Mon. Weather Rev.*, *117*, 1751–1766, doi:10.1175/1520-0493(1989)117<1751:SEOTFG>2.0.CO;2.

Susskind, J., P. Piraino, L. Rokke, L. Iredell, and A. Mehta (1997), Characteristics of the TOVS pathfinder path a data set, *Bull. Am. Meteorol. Soc.*, *78*, 1449–1472, doi:10.1175/1520-0477(1997)078<1449:COTTPP>2.0.CO;2.

Wylie, D., and W. Menzel (1999), Eight years of high cloud statistics using HIRS, *J. Clim.*, *12*, 170–184.

Zhang, M., et al. (2005), Comparing clouds and their seasonal variations in 10 atmospheric general circulation models with satellite measurements, *J. Geophys. Res.*, *110*, D15S02, doi:10.1029/2004JD005021.

H. Joos, U. Lohmann, and P. Spichtinger, Institute for Atmospheric and Climate Science, ETH Zurich, Universitaetstrasse 16, CH-8092 Zurich, Switzerland. (hanna.joos@env.ethz.ch)